

Global CO₂ transport simulations using meteorological data from the NASA data assimilation system

S. R. Kawa,¹ D. J. Erickson III,² S. Pawson,^{3,4} and Z. Zhu⁵

Received 19 January 2004; revised 21 June 2004; accepted 12 July 2004; published 29 September 2004.

[1] We present a first analysis of atmospheric CO₂ transport using meteorological data from the NASA finite volume data assimilation system (FVDAS). The analyzed meteorological fields are used along with climatological surface sources and sinks in an off-line, forward transport simulation for 1998–2000. Analysis of model diagnostics and comparisons to previous results indicates that the model performance is consistent with that of most previous global transport models. The model interhemispheric gradients along with the timing and magnitude of the CO₂ seasonal cycle are discussed, providing inferences regarding the northern biosphere, tropical land, and southern ocean fluxes. Global distributions of column-integrated CO₂ are presented to provide a basis for measurement requirements for the design of satellite-based instruments for atmospheric CO₂ column. On the synoptic scale we find a significant benefit in using the FVDAS analyzed winds for comparisons to data. At near-equatorial observation sites, the model correctly simulates the observed atmospheric composition transition associated with the latitudinal movement of the ITCZ. Comparison to daily data from continuous analyzer sites shows the model captures a substantial amount of the observed synoptic variability due to transport changes. These results show the potential to use high temporal and spatial resolution remote sensing data to constrain CO₂ surface fluxes, and they form the starting point for developing an operational CO₂ assimilation system to produce high-resolution distributions of atmospheric CO₂ and quantitative estimates of the global carbon budget. *INDEX TERMS*: 0315 Atmospheric Composition and Structure: Biosphere/atmosphere interactions; 0322 Atmospheric Composition and Structure: Constituent sources and sinks; 0368 Atmospheric Composition and Structure: Troposphere—constituent transport and chemistry; 3337 Meteorology and Atmospheric Dynamics: Numerical modeling and data assimilation; *KEYWORDS*: carbon dioxide, data assimilation

Citation: Kawa, S. R., D. J. Erickson III, S. Pawson, and Z. Zhu (2004), Global CO₂ transport simulations using meteorological data from the NASA data assimilation system, *J. Geophys. Res.*, 109, D18312, doi:10.1029/2004JD004554.

1. Introduction

[2] CO₂ emissions, primarily from fossil fuel burning, are the largest anthropogenic climate driver and will be for the coming decades to centuries [Intergovernmental Panel on Climate Change (IPCC), 2001]. In order to make accurate projections of future atmospheric CO₂, we need to understand what controls the highly variable atmospheric CO₂ concentrations, the role of various surface sources and sinks in the global carbon cycle, and the mechanisms through which CO₂ sources and sinks interact with changing climate. Currently, significant uncertainties are attached to our

understanding of these processes [IPCC, 2001; Schimel *et al.*, 2001]. Resolving these issues is critical to reliable predictions of future climate forcing and effective remedial/preventative actions.

[3] The global distribution of CO₂ surface fluxes is commonly inferred from transport models and atmospheric concentration measurements (inverse modeling) [Enting and Mansbridge, 1991; Fan *et al.*, 1998; Bousquet *et al.*, 1999]. This approach is limited by the accuracy of the numerical transport model, the circulation/wind inputs that drive the transport, and the observational CO₂ data. Transport model differences have been a major source of variation in the inference of CO₂ sources and sinks [Law *et al.*, 1996; Denning *et al.*, 1999; Gurney *et al.*, 2002; Peylin *et al.*, 2002]. The TransCom project [Gurney *et al.*, 2002, and references therein] is an international effort to quantify the errors introduced into our understanding of the carbon cycle by differences/errors in the circulations and transport computed by models. The work reported here uses the transport core and meteorological analyses from a state of the art data assimilation system to produce 3-D atmospheric CO₂ distributions based on TransCom emission scenarios.

¹NASA Goddard Space Flight Center, Greenbelt, Maryland, USA.

²Oak Ridge National Laboratory, Oak Ridge, Tennessee, USA.

³Goddard Earth Science and Technology Center, Baltimore, Maryland, USA.

⁴Also at Global Modeling and Assimilation Office, NASA Goddard Space Flight Center, Greenbelt, Maryland, USA.

⁵Science Systems and Applications, Inc, Lanham, Maryland, USA.

[4] The motivation for studying CO₂ transport with assimilated winds is based on the ability of such fields to realistically represent synoptic to global scale, real-time variability while maintaining internal dynamical consistency in time and space. This allows real-time, point-by-point comparisons to data, rather than merely climatological comparisons. This advantage will become more significant as data coverage increases, e.g., with space-based remote sensing of atmospheric CO₂. Here we analyze results of CO₂ simulations in a transport model across a wide range of timescales using the assimilated meteorological fields from the NASA Goddard Global Modeling and Assimilation Office. Even with assimilated winds, however, we do not expect to exactly reproduce the measured CO₂ time series because we are still using climatological surface fluxes.

[5] The overall objective of this work is to present a first analysis of atmospheric CO₂ transport using meteorological data from the finite volume data assimilation system (FVDAS). We use the model results and comparisons to data in two primary tasks. The first is to characterize the model transport using climatological CO₂ sources and sinks. This task sets the foundation for using this model in an inverse mode to deduce surface source/sink relationships and establishes the baseline for testing improved representations of model processes. It also serves to document the use of the model as a test bed with realistic gradients and variability for developing remote sensing measurement requirements and retrieval algorithms for potential space-based CO₂ instrumentation [e.g., Mao and Kawa, 2004].

[6] A second task is to use this model to evaluate constraints on the atmospheric CO₂ budget discernable in forward mode. Forward modeling studies have addressed many of the main atmospheric CO₂ budget issues using estimates of atmospheric circulation derived from climate models [Fung et al., 1983; Denning et al., 1995; Erickson et al., 1996; Randerson et al., 1997] and analyzed winds [Heimann and Keeling, 1989; Taguchi, 1996; Bousquet et al., 1999, 2000]. Here we summarize relevant model progress since Erickson et al. [1996] and assess the impacts of new terrestrial biological fluxes, ocean CO₂ flux, and an alternative treatment of the biomass burning source of CO₂. We compare computed CO₂ distributions to local and global observations on daily to interannual timescales to assess the reliability of the surface source/sink formulations and to evaluate the contribution of meteorological variability to the observed CO₂ distributions. This type of analysis should eventually lead to a more sophisticated description of sources/sinks at higher time and spatial resolution. In addition, such evaluation is a first step toward assimilating high-resolution CO₂ data into global models.

[7] We organize the results reported here by a hierarchy of temporal scales. We find that overall the model large-scale transport characteristics are consistent with previous model intercomparisons. The model does an outstanding job of simulating the seasonal cycle of atmospheric CO₂ at various globally distributed stations and the dynamical component of synoptic-scale variability associated with specific features of the atmospheric circulation such as storm patterns and the movement of the ITCZ. The inter-hemispheric gradient of CO₂ and the annual increase

(considering land use change) is overestimated, consistent with most models lacking the NH “missing sink” [Tans et al., 1990; Denning et al., 1995; Fan et al., 1998]. Interannual variability in circulation contributes little to large-scale CO₂ changes at most sites.

[8] Section 2 provides a description of the transport model, the FVDAS, and model evaluation tests. Section 3 discusses the global CO₂ distributions from the model. Section 4 focuses on comparisons with data, section 5 discusses future work, and section 6 presents a summary of significant findings.

2. Chemistry Transport Model

2.1. Model Description

[9] The GSFC parameterized chemistry and transport model (PCTM) used for the CO₂ forward simulations in this study has been adapted from an established full-chemistry/transport model [e.g., Douglass and Kawa, 1999; Douglass et al., 2003; Nielsen and Douglass, 2001]. At the core of the PCTM is the transport code of Lin and Rood [1996], which is formulated in flux form and adopts a semi-Lagrangian algorithm. The accuracy of this code for large-scale transport is well documented for test studies [Lin and Rood, 1996], large-scale stratospheric dynamics [Douglass et al., 2003] and for long-range tropospheric chemistry/transport studies [e.g., Li et al., 2002]. For studies of tropospheric trace gases, including carbon species, it is necessary to include transport due to subgrid-scale processes such as convection and boundary layer diffusion. The PCTM can be driven by meteorological fields from model simulations or meteorological analyses. In this study, it is driven by analyzed meteorological fields from a prototype version of NASA’s Goddard Earth Observation System, version 4 (GEOS-4) data assimilation system (DAS).

[10] The GEOS-4 analysis system is built around the so-called finite-volume general circulation model (FVGCM) and the physical space statistical analysis scheme (PSAS) [Cohn et al., 1998]. The prototype version of GEOS-4 used in this study was referred to as the FVDAS, and this name will be retained in this manuscript in order to identify it as a preoperational version of the system. A suite of observations is input into FVDAS, including in situ meteorological products (radiosondes, aircraft measurements), and satellite data (e.g., TIROS Operational Vertical Sounder (TOVS) level-1b radiances [after Joiner and Rokke, 2000], cloud track winds, total precipitable water, and surface winds). The cycling of the FVDAS is in 6-hour windows, using the observations within ± 3 hours of the analysis time and a 6-hour FVGCM forecast.

[11] The FVGCM is based on the Lin-Rood dynamical core [Lin and Rood, 1996]. Physical tendencies are determined using the National Center for Atmospheric Research (NCAR) Community Climate Model, Version 3 (CCM3) package [Kiehl et al., 1998]. This includes the deep convection code of Zhang and McFarlane [1995], shallow convection determined from Hack [1994], and planetary boundary layer (PBL) turbulence [Holtslag and Boville, 1993].

[12] The assimilation process produces the meteorological variables (horizontal winds, surface pressure, temperature, moisture), yielding optimally analyzed fields at 6-hour res-

olution. Additional variables that are produced by the model are saved as 6-hour averages including the cloud mass fluxes and turbulence parameters necessary to drive the CTM. A further uncertainty with using assimilated products for tropospheric constituent studies is the nonconservation of mass; this arises from local mass adjustments in the assimilation process and the absence of a global constraint, because of the sparsity of data. Note that the free-running FVGCM conserves mass. Note also that, in the mean, there is no net accumulation or loss of mass in the FVDAS (a consequence of the errors being random and the long-term global coverage of the observations). This local nonconservation of mass does, however, necessitate the introduction of an additional “pressure fixer” procedure in the PCTM, which is discussed below (section 2.3).

[13] The PCTM was run using FVDAS output for the 1998–2000 period, run at 2.5° by 2° (longitude by latitude) with 55 hybrid vertical levels. The CTM used the same horizontal resolution, but with 25 levels up to 1 mbar, of which 14 are below 175 mbar. A divergence-conserving vertical interpolation scheme was used to remap the wind data [Douglass and Kawa, 1999]; stratospheric levels are combined for computational efficiency. CO₂ is treated as a passive constituent (within the range of interest for this study). The small source from CO oxidation is assumed to be included in the surface emissions. Thus the CO₂ distribution is determined only by transport from the specified sources and removal at the surface sink regions.

2.2. Distributions of CO₂ Sources and Sinks

[14] The surface sources and sinks of CO₂ are largely based on the compilations used in TransCom 3 [Gurney *et al.*, 2002]. Sources and sinks associated with the terrestrial biosphere are based on computations of net primary productivity from Randerson *et al.* [1997]. Ocean sources and sinks are adopted from Takahashi *et al.* [1999], an updated version of Takahashi *et al.* [1997], which display strong seasonal variations, unlike those from earlier estimates [e.g., Erickson *et al.*, 1996]. Estimates of fossil fuel emissions are from Andres *et al.* [1996] for 1990 (global total = 5.8 Pg C yr⁻¹). Finally, an additional source is used to estimate CO₂ gradients produced by land use change. Surface CO₂ fluxes are produced from monthly spatial distributions of biomass burning for 1998–2000 [Duncan *et al.*, 2003], and scaled to an annual total emission of 1 Pg C to simulate a net land use change flux.

[15] The surface sources and sinks used in this study represent diurnal averages compiled into monthly means. Use of average fluxes will affect the simulations in several ways. First, it damps the computed diurnal cycle of biospheric CO₂ in the PBL, especially in the source/sink regions. Through interactions with vertical convective transport and PBL venting, there may be an impact on the amount of CO₂ transported into the free atmosphere, where it can subsequently be transported over large horizontal distances [Denning *et al.*, 1995]. Second, the PBL depth and ventilation, as well as the cloud mass fluxes, can themselves have errors in their diurnal cycles, which could also result in similar problems. These two factors, which could interact in complex ways, will be the subject of future examination; the uncertainties involved justify the use of the daily mean surface fluxes at this stage of model development. Also, the

6-hour mean transport parameters are not adequate to resolve the diurnal cycle of the planetary boundary.

2.3. Model Evaluation Tests

[16] We have made considerable effort to ensure the model’s numerical accuracy. The global total mass of CO₂ should not change during transport since the tracer mass is only redistributed, however, we found tracer was not conserved with the initial offline model during advection and convection. The source of the error in advection lies in application of the DAS meteorological data in which the surface pressure tendency and the mass flux convergence are not always consistent. This inconsistency causes a mismatch between the predicted and the data-based surface pressure at the next time step. Therefore the total mass of a tracer is not conserved during the advection process, causing errors in the simulated tracer field. Prather *et al.* [1987] first revealed this kind of numerical error in a CTM, and tried to fix it by modifying the wind data. A similar method of using a pressure fixer has been developed recently at the Lawrence Livermore National Laboratory (LLNL) [Rotman *et al.*, 2001]. The LLNL pressure fixer removes the global and zonal mean pressure errors and subsequently the zonally distributed errors. In the vertical, the changes of mass flux are proportional to the sigma coefficient, so that it does not induce a vertical wind change. We introduced the LLNL pressure fixer into our PCTM and found that it can precisely remove the inconsistency of the wind and surface pressure data and also is computationally efficient.

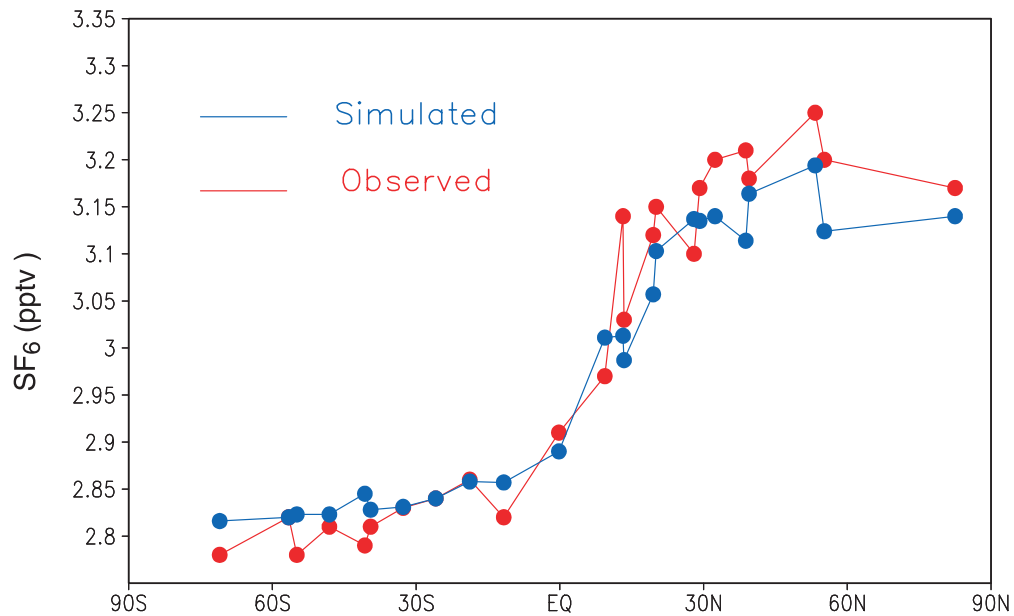
[17] We also implemented a new mass conserving, semi-implicit convective transport module, constrained by the subgrid-scale fluxes from the assimilation system. The procedure is designed to be consistent with the deep convection scheme used in the FVGCM [Zhang and McFarlane, 1995]. Vertical cloud transport is calculated according to the following:

$$q_k^{t+\Delta t} - q_k^t = \frac{g\Delta t}{\Delta p_k} [C_{k+1}(q_{k+1} - q_k) - C_k(q_k - q_{k-1})]^{t+\Delta t/2}$$

where q is the tracer concentration, C_k and C_{k+1} are the net convective mass flux at the upper and lower edges of layer k , t is the model time step, and $\Delta p_k/g$ is the air mass of the layer. The quantities q on the right side of the equation are taken at the middle of the time step, which is expressed as the mean of the right side at the current and next time step, $t + \Delta t/2$. An implicit scheme is then used to solve the equation.

[18] The above model procedures have a significant effect on the off-line transport. In the original formulation, the maximum seasonally dependent error was about 20% of the annual CO₂ mass increase due to emissions. With the updated model, however, the total CO₂ mass increase is exactly equivalent to the surface emission. The mass change due to convection is the major fraction of the difference, except in August–October when the pressure fixer dominates the change. The results show a significant difference in the simulated interhemispheric gradient, which is reduced from almost 8 ppmv to 6 ppmv in the improved model. This change is a good example of how atmospheric CO₂ simulations depend on the accuracy of the transport models and the meteorological data.

[19] In order to verify the quality of the transport model and the computed circulation data, we conducted a sulfur hexafluoride (SF₆) simulation experiment following the



Annual mean surface layer SF₆ mixing ratio (pptv)

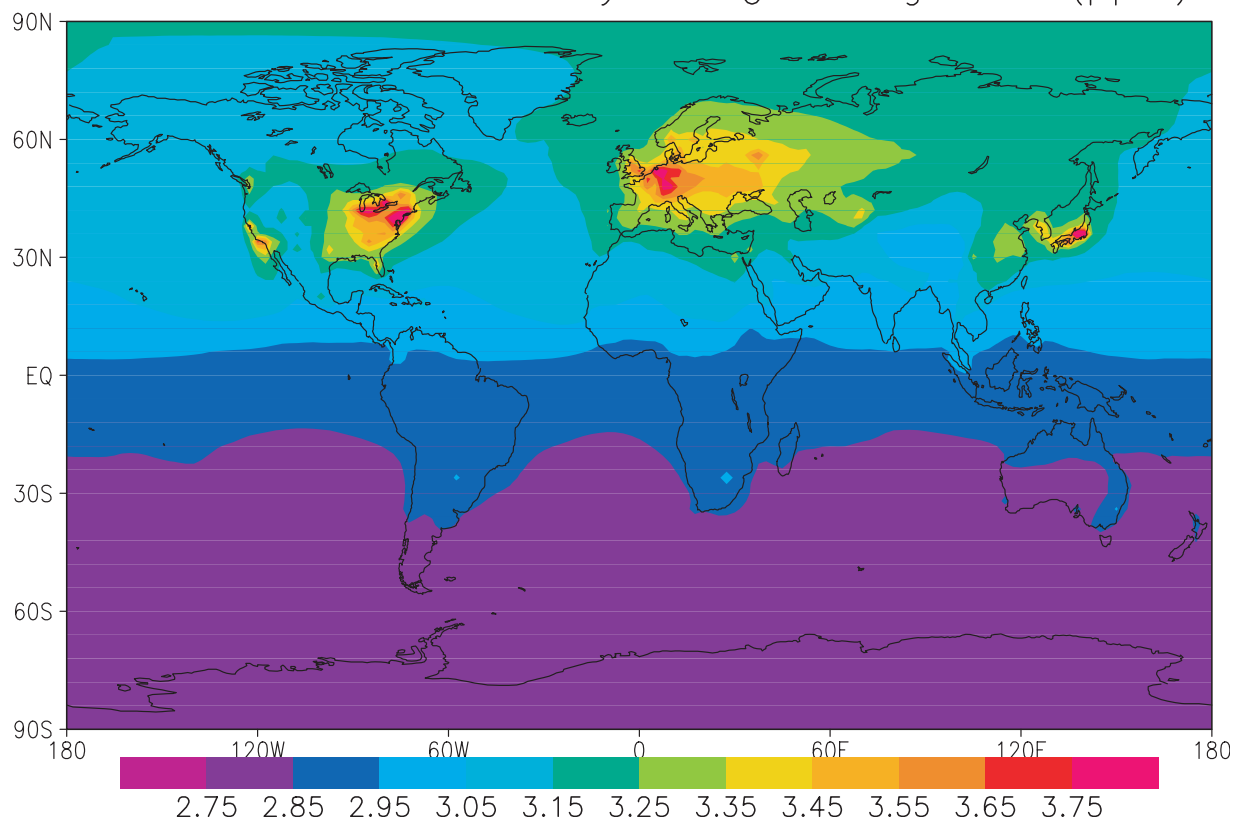


Figure 1. (top) Annual mean SF₆ (pptv) as a function of latitude interpolated from the model and observed at 24 locations from *Denning et al.* [1999]. (bottom) Annual mean distribution of SF₆ at the model surface.

procedure of TransCom 2 [*Denning et al.*, 1999]. Comparison of the simulated annual mean SF₆ concentration at 24 stations, all in the marine boundary layer, as a function of latitude (Figure 1) reveals that the simulated meridional gradient is generally consistent with the observations,

although it is underestimated by about 0.1 pptv. Compared to Figure 3 from *Denning et al.* [1999], this result is consistent with the models in TransCom 2.

[20] The Figure 1 (bottom) shows the simulated annual mean surface layer SF₆ concentration (pptv). The global

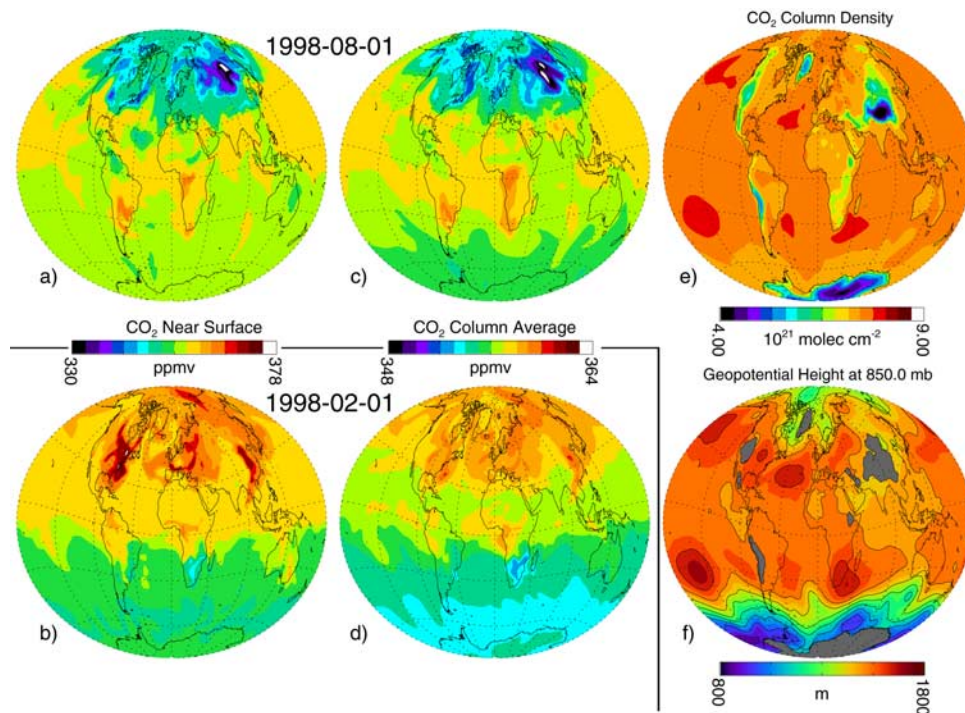


Figure 2. (a and b) CO₂ mixing ratio near the surface (~ 900 mbar) and (c and d) CO₂ column average (note color scale change). The top panels are for 1 August 1998, and the bottom panels are for 1 February 1998. Also shown are (e) CO₂ column density and (f) geopotential height at 850 mbar for 1 August 1998. All frames are taken at 0000 UT. The column average CO₂ is found simply by dividing the column density by surface pressure in appropriate units.

mean surface concentration is 2.97 pptv, which is in the middle of the estimates from other models that range from 2.94 to 3.01 pptv [Denning *et al.*, 1999]. The simulated SF₆ concentration values in some major surface source regions are quite close to the observations. For example, the simulated SF₆ at a Hungarian station (47°N, 16°E), a Wisconsin site (46°N, 90°W), and the Tae Ahn Peninsula (37°N, 126°E) are 3.67, 3.34, and 3.39 pptv respectively, while the observed values in these locations are 3.42, 3.31, and 3.25 pptv. The simulated values are only slightly overestimated. We also estimated the 3D interhemispheric transport exchange time defined by Denning *et al.* [1999]. The value is 0.61 years, which is comparable to the faster ones in TransCom 2. This may imply that the vertical mixing in the present model is greater than that of most models in TransCom 2. The surface maxima of about 3.7 pptv in the source regions (Figure 1, bottom), however, are in the middle of the range of TransCom 2 results so vertical mixing is not extreme by this measure. These diagnostics will help to guide future model development efforts. We conclude, based on our analyses of the tracer transport and model diagnostics, that this model compares well to other chemical transport models used in earlier intercomparisons.

3. Modeled Global CO₂ Distributions

[21] We present several examples of global CO₂ distributions calculated by the forward model for the purpose of quantifying the expected gradients of atmospheric CO₂ that exist in response to surface forcing. Such distributions are needed to formulate measurement requirements and retrieval

approaches for potential space-based remote sensors for atmospheric CO₂. The spatial distributions of CO₂ in the model reflect the climatological surface fluxes, modulated by transport in wave structures that can be observed in the geopotential height fields (Figure 2f). The general characteristics of the computed CO₂ distributions, such as regional horizontal gradients near the surface and CO₂ column average are shown in snapshots from two different seasons in Figure 2 along with an example plot of CO₂ column density and geopotential height for August.

[22] Comparison of CO₂ near the surface on 1 February and 1 August highlights the clear signature of the seasonal cycle in CO₂ that is induced mainly by the terrestrial biosphere flux. Figure 3 shows typical profile changes as a complement to the near-surface changes in Figure 2. Profiles from several example sites (Figure 3) show that the largest CO₂ seasonal variability occurs in the lower troposphere in close proximity to the surface sources and sinks. The CO₂ profiles are nearly constant above the planetary boundary layer (PBL) and away from active source/sink regions where advective transport plus mixing through convection and diffusion damps the surface effects. In reality, there is a strong diurnal cycle superimposed on the CO₂ seasonal cycle over vegetation in the growing season. In the model there is no diurnal cycle in the fluxes so the diurnal cycle of CO₂ is relatively weak. For comparisons to data below we use measured daily average CO₂ and samples from sites not immediately affected by the vegetation diurnal cycle. Future realizations of the model will include diurnally varying biosphere fluxes and a more complete representation of the diurnal cycle in transport.

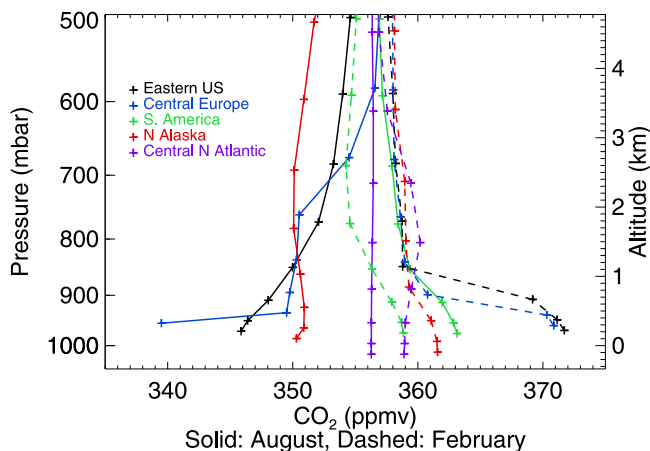


Figure 3. Vertical distribution of the CO₂ mixing ratio (ppmv) as a function of pressure in selected regions on 1 February 1998 (dashed line) and 1 August 1998 (solid line) at 0000 UT. Pluses show the resolution of the model vertical levels. Altitude scale is approximate pressure altitude.

[23] Advances in carbon science, and CO₂ budgets in particular, are expected to be made using satellite measurements of atmospheric CO₂ in the relatively near future [e.g., Rayner and O'Brien, 2001; Pak and Prather, 2001]. In order to observe the near-surface variability of CO₂ from space, a near-nadir total column CO₂ measurement is generally thought to be most feasible [Kuang et al., 2002]. The column-average mixing ratios (Figure 2) show that variations in the column generally reflect the changes in near-surface CO₂. The column gradients are on the order of a few ppmv per 1000 km. This represents an estimate of the minimum level of precision required for a satellite instrument to resolve CO₂ changes related to surface forcing. Similar precision requirements have been obtained from inverse modeling [Rayner and O'Brien, 2001; Pak and Prather, 2001]. Total CO₂ column density from the model, however, such as would be directly measured by optical absorption (e.g., the Total Ozone Mapping Spectrometer [McPeters and Labow, 1996]) reveals that variations in terrain height and surface pressure (i.e., weather systems) create gradients larger than those from CO₂ surface fluxes (Figures 2e and 2f). A method for normalizing the measured CO₂ column density to account for varying absorption path is needed, for example through simultaneous measurement of O₂ column [O'Brien and Rayner, 2002]. The ability of the transport model used to track the influence of surface forcing at different altitudes and times will be very important to correctly interpret CO₂ column abundances in relation to surface fluxes.

[24] As a sensitivity test to examine potential variability of the CO₂ column mixing ratio, an additional source of 1 Pg C/yr due to land use change, distributed in the horizontal like biomass burning, was included as a separate tracer. This source resulted in a 0.5-ppmv/yr global increase in total column CO₂ with a mean column gradient (not shown) of about 0.3 ppmv increasing from high to low latitudes (see Figures 2c and 2d). This difference in global column CO₂ with and without an explicit biomass burning/land use source is an example of the magnitude of column

variation that needs to be detectable on a global scale for monitoring and attribution.

[25] Several other characteristics of the transport model performance can also be compared in the global fields. The annual average vertical difference between the surface and 500 mbar of fossil-fuel CO₂ (not shown) is similar to the mean of models for TransCom 1 shown in Figure 5 of Law et al. [1996]: the NH maximum is 2 ppmv and the minimum in the SH is -0.5 ppmv. The computed CO₂ concentration at 200 mbar has a magnitude and pattern similar to data [Nakazawa et al., 1991] and Figures 6 and 7 of Law et al. [1996] with a maximum in the subtropics.

4. Analysis of Results in Comparison to Data

[26] We evaluate the FVDAS-based simulations of atmospheric CO₂ by comparing the computed distributions with observations across a range of temporal and spatial scales. We start with the larger-scale variations, such as the interhemispheric gradient of atmospheric CO₂, which is strongly influenced by the large-scale transport but is also linked to convective and turbulent processes. Then we examine the seasonal cycle of atmospheric CO₂ as a function of latitude, compare to data time series at specific sites, and comment briefly on trends. We finish the model evaluation by examining the synoptic-scale variability of CO₂ in the model that reflects daily changing DAS meteorology.

4.1. Interhemispheric Gradients

[27] The interhemispheric CO₂ gradient in the simulations presented here is composed of annual-averaged contributions from the four source/sink components (Figure 4). The fossil fuel CO₂ gradient is within the range of models from Law et al. [1996], although perhaps toward the lower quartile, considering the total fossil flux difference between

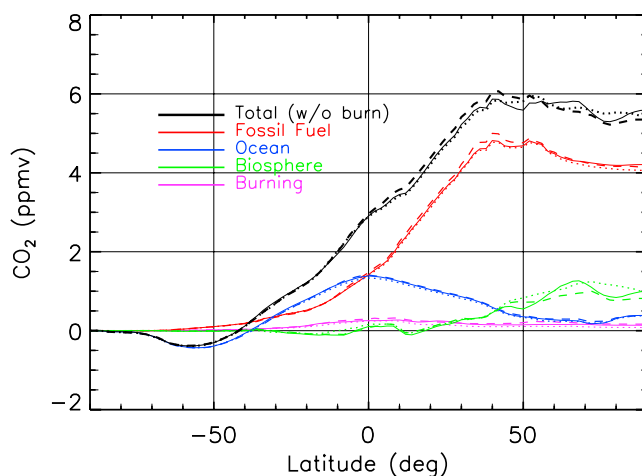


Figure 4. Interhemispheric gradients of atmospheric CO₂ at the surface (lowest model level) from the different individual source/sink terms used in the simulations (fossil fuel, ocean, terrestrial biosphere, and biomass burning) as well as the total. The annual zonal means from three years are shown: 1998 (dashed line), 1999 (solid line) and 2000 (dotted line), minus the mixing ratio at South Pole. The biomass burning/land use change term is not included in the total for consistency with other plots.

the experiments that is a factor of 1.09 larger here. The hemispheric concentration difference is 3.6 ppmv (3.1 ppmv scaled to emission), which is consistent with our finding from the SF₆ experiments (above) that this model has relatively fast interhemispheric exchange. Comparison to TransCom 3 results [Zhang 2003] yields similar conclusions. The biosphere gradient is intermediate to the examples of Denning *et al.* [1995] and less than those of Erickson *et al.* [1996], demonstrating a significant effect of the seasonal “rectifier” that results from seasonality in the terrestrial biosphere that covaries with the seasonality in interhemispheric transport [Denning *et al.*, 1995]. In interpreting these comparisons, one should note that the treatment of the terrestrial biosphere fluxes is different between the model runs as well as the model specific transport characteristics. Comparison to TransCom 3 shows this to be one of the less strong rectifier models [Gurney *et al.*, 2003].

[28] Figure 4 shows that small interannual differences in the model total CO₂ mean gradient arise mainly from the biosphere component. This means that the interannual variations in transport affect the correlation of transport with the seasonal cycle in emissions/uptake, i.e., the seasonal rectifier. Observed interannual variability of atmospheric CO₂ reflects variability in both the surface source/sinks and the circulation patterns (such as the influence of El Niño or the North Atlantic Oscillation). The ability to capture some interannual variability through transport alone shows a potential advantage of using the DAS for the transport calculations as opposed to a climatological circulation or GCM fields for real-time comparison with data.

[29] The interhemispheric gradient compared to observations (Figure 5) has implications for carbon cycle processes and modeling. The model overestimate of the gradient (Figure 5 does not include the burning/land use source) and the rate of annual increase (discussed below) imply an additional NH sink of magnitude $\sim 1.2 \text{ Pg C yr}^{-1}$ is needed, as has been inferred in previous work [Tans *et al.*, 1990; Denning *et al.*, 1995]. Interannual variation in the interhemispheric gradient is significant in data but small in the model, which implies that atmospheric transport variation is not a major influence, and that the actual surface fluxes must be varying significantly from year to year [cf. Dargaville *et al.*, 2000]. Interannual variability of CO₂ gradients is correlated with climate variability, e.g., El Niño, primarily through the influence on ocean and terrestrial CO₂ fluxes [Rayner *et al.*, 1999; Schimel *et al.*, 2000; Bousquet *et al.*, 2000].

[30] The biomass burning/land use source as input here accentuates the Northern Hemisphere excess by about 0.5 ppmv (Figure 4) since more of the effluent goes to the north. There is little interannual variation for modeled CO₂ from the burning source in these years, in spite of large differences in the global horizontal distribution of burning, especially in the tropics. It is also important to note that most of the observational sites are not located well to pick up tropical burning plumes and only see the mean increase as in Figure 4. The source is rapidly transported vertically in tropical convection and has little influence on surface CO₂ outside the active region. On the basis of this simulation, interannual changes in the global magnitude of the burning/land use may be detectable, but changes in the spatial pattern of emissions will be difficult to detect using present

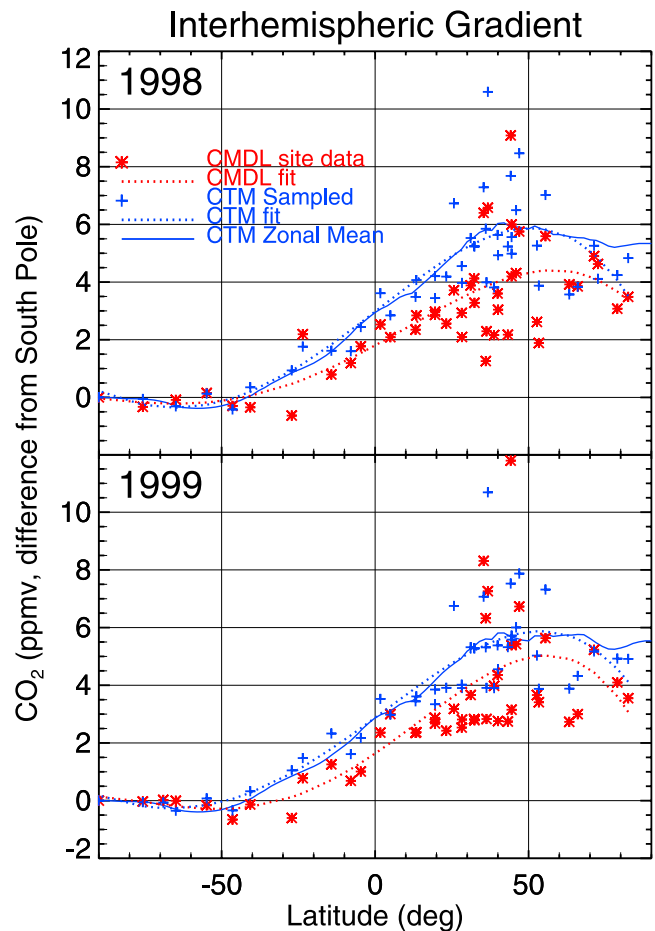


Figure 5. Comparison of the annual mean latitude gradient of atmospheric CO₂ from the model (blue) and observations (red) for 1998 and 1999. Individual sites (symbols) are shown along with a polynomial fit over latitude of the observations and model sampled to the observation points (dotted lines). The model zonal mean from all grid points is the solid line. Figure 5 includes the fossil fuel, ocean, and biosphere model components.

surface CO₂ observations, since vertical transport and mixing is generally large in tropical areas.

4.2. Latitude Distribution of the Seasonal Cycle

[31] The local magnitude of the atmospheric CO₂ seasonal cycle is dependent on a variety of factors in the general circulation. Proximity to strong sources or sinks, the time-scale of transport from sources/sink regions relative to diffusion of atmospheric CO₂ concentration gradients, and details of convection, boundary layer processes, and advective transport all influence the seasonal cycle of atmospheric CO₂. Figure 6 compares the amplitude of the seasonal cycle of atmospheric CO₂ in the model with observations [Conway *et al.*, 1988] at numerous stations for the same times (1998 and 1999). Results for 2000 are very similar to 1999. The modeled CO₂ amplitude (Figure 6) and phase (Figures 7 and 8a–8e) in the NH is generally in close agreement with observations [cf. IPCC, 2001]. The amplitude of the seasonal cycle globally is driven mainly by the biological flux cycle from the continents, with a modest

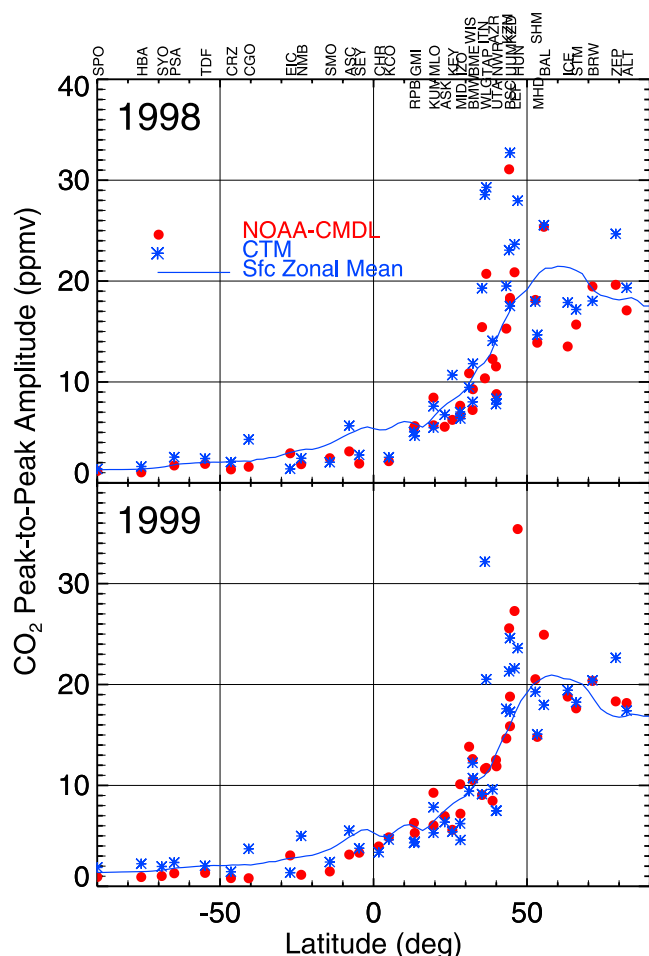


Figure 6. Amplitude of the seasonal cycle of atmospheric CO₂ as a function of latitude for 1998 and 1999. The red dots are flask observations, and the blue stars are from the model daily mean output (not including the biomass burning source). The seasonal amplitude for each year is calculated from the peak-to-peak difference in the time series with the linear trend removed and a five-point triangular smoothing filter applied. Also shown is the zonal mean of the amplitudes of the model monthly means (blue line).

ocean forcing that reinforces the biospheric cycle near strong ocean sink regions. In the SH middle to high latitudes, the ocean contribution to the seasonal amplitude is comparable to that from the terrestrial biosphere cycle. The NH phase (Figures 7 and 8a–8e) is good, better than that of *Erickson et al.* [1996], and there is significant improvement over the simulations compared by *Law et al.* [1996]. This supports the realism of the *Randerson et al.* [1997] biosphere fluxes used here. There is little interannual variability in the seasonal amplitude in the model but it agrees more closely with data for 1998 in the Southern Hemisphere than in other years because the observed seasonal cycle is larger. This may be the result of enhanced CO₂ emission from biomass burning in 1998 [*Langenfelds et al.*, 2002] and shows again the potential benefit of constraining fluxes by comparing model and data for specific time periods.

[32] The seasonal cycle at individual sites shows some large differences from the zonal mean especially from 30 to

50°N. Large CO₂ amplitude at these sites is usually caused by the effect of the local continental biosphere and/or urban pollution and is generally seen in both the observations and the model. Enhancement of the present observational network is required to better characterize the global seasonal carbon balance. The largest differences between modeled and observed amplitude (Figure 6) are seen at sites for which the measurements are selected for background conditions to screen out large local influence (e.g., TAP, WLJ, CGO) or only limited data are available (e.g., ICE in 1998, UUM, NMB). In other cases the comparison suggests real variations in the seasonal cycle not captured by the climatological flux distribution (e.g., ZEP, BAL in summer of 1999 (Figure 7), HUN).

4.3. Flask Site Comparisons

[33] We have selected several sites across a wide range of latitudes for a direct time series comparison between the model and the CMDL data. Figure 7 shows the time series of computed atmospheric CO₂ concentrations at eight sites compared to flask observations [*Conway et al.*, 1988]. Additional time series are shown in Figures 8a–8e in comparison to daily mean data from continuous analyzer data [*Thoning et al.*, 1989; *Bakwin et al.*, 1998]. We arrange the discussion of results in the order of regional signatures from the North Pole to the South Pole.

4.3.1. Northern Middle to High Latitudes

[34] The amplitude, phase, and to some extent the interannual variability in the seasonal cycle at northern middle to high latitudes are quite well simulated (e.g., ALT, SHM, BRW, IZO) as far south as about 28°. The model also captures the fact that synoptic-scale, week-to-week variability is greater at sites more strongly influenced by local source or sinks (e.g., Figure 7, BAL). In addition to confirming the overall quality of the climatological biosphere flux seasonality and horizontal distribution, these comparisons indicate that the transport processes are reasonably well simulated.

4.3.2. Subtropics and Tropics

[35] Variations in meteorology are well simulated in many cases, such as the seasonal latitudinal movement of the Intertropical Convergence Zone (ITCZ) (e.g., CHR, SEY). One can see the sudden shift in influence from the NH to SH at CHR and SEY as the ITCZ moves north and the atmospheric CO₂ concentration drops to levels typical of the Southern Hemisphere. Eventually one may be able to use this higher temporal resolution data to better constrain surface source/sink estimates in inversions. This is also an example where satellite data could contribute to better representing the time evolution of atmospheric CO₂ distributions that can concurrently take advantage of DAS analyzed winds.

[36] The computed summer minimum at most sites South of about 28°N, e.g., ASK, MLO, is underestimated by the model. This suggests too little uptake in the sub-Saharan terrestrial biosphere during this time period or perhaps too little advection of CO₂ depleted air masses from the Northern Hemisphere mid latitudes. The vertical gradient of CO₂ and the vertical damping of the seasonal cycle is well replicated in comparison to surface and elevated sites in Hawaii (not shown, KUM and MLO) and IZO indicating that the vertical transport parameterization is reasonable [cf.

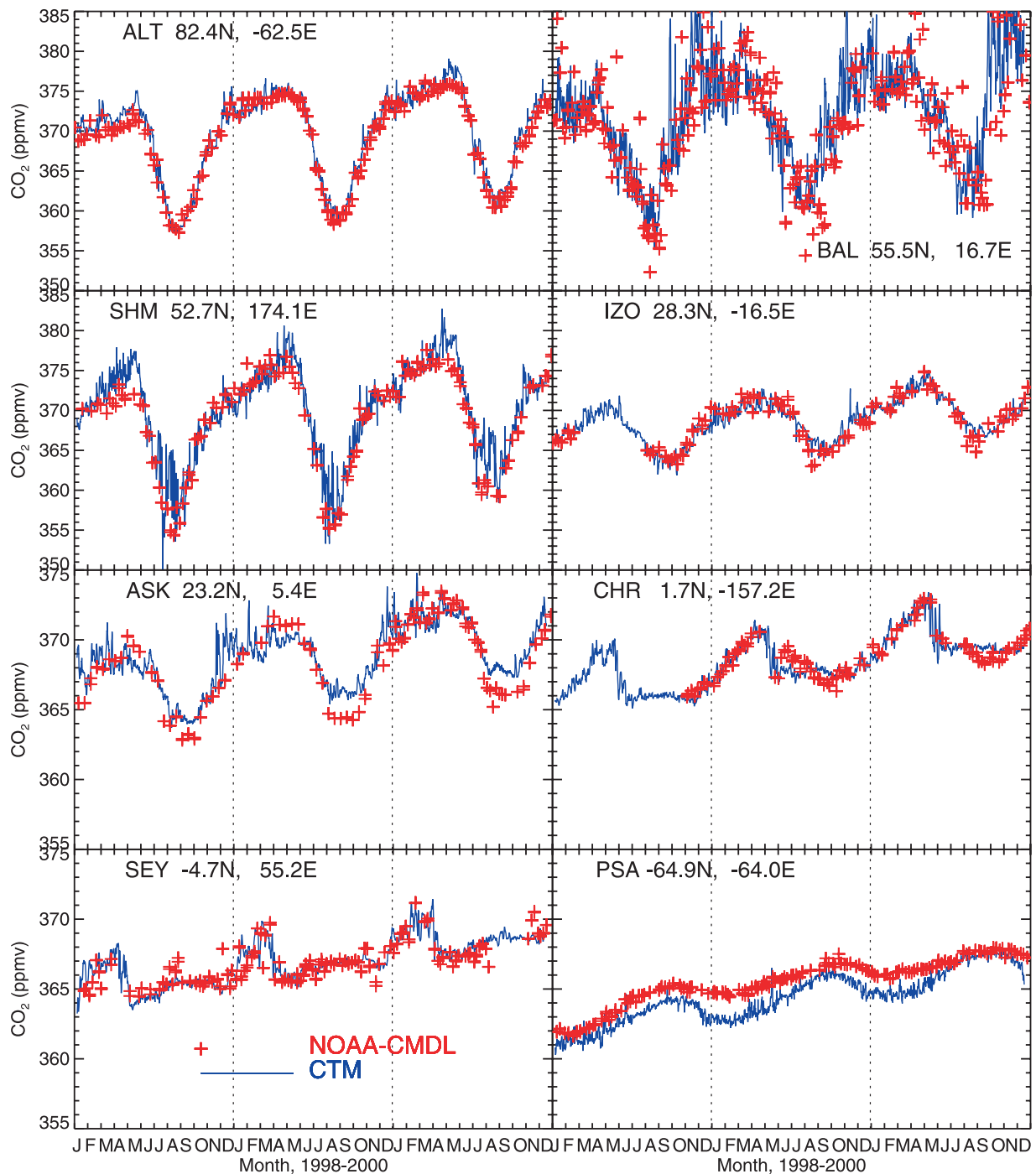


Figure 7. Time series of atmospheric CO₂ for 1998–2000 for eight NOAA/CMDL surface stations (red pluses) and comparison to model at the same locations (blue line). Flask samples are taken roughly once a week near local noon, and the model output is the daily mean. Model mixing ratios are the total of the fossil, ocean, and biosphere CO₂ globally offset so the 3-year mean at Mauna Loa equals that of the observations. Data are from version current at December 2001.

Erickson et al., 1996]. Our comparisons to data at northern latitudes and tropics generally look better than those of *Randerson et al.* [1997], who used the GISS tracer model. This may be a result of different transport characteristics in the present model due to improved model formulation and/or the use of assimilated winds.

[37] The simulated biomass burning/land use source contribution to the magnitude ($\ll 1$ ppmv) and timing of the

seasonal cycle is negligible at most flask sites. The tropical Africa and Indian Ocean sites NMB, KCO, and SEY in 1998–2000, and BRW in 1999 are the exceptions at ~ 1 ppmv, which can be compared to the total amplitudes in Figure 6. As discussed above, most observational flask sites aren't positioned to see the effect of biomass burning. This is a different conclusion than that of *Randerson et al.* [1997] whose biomass burning contributes substantially to

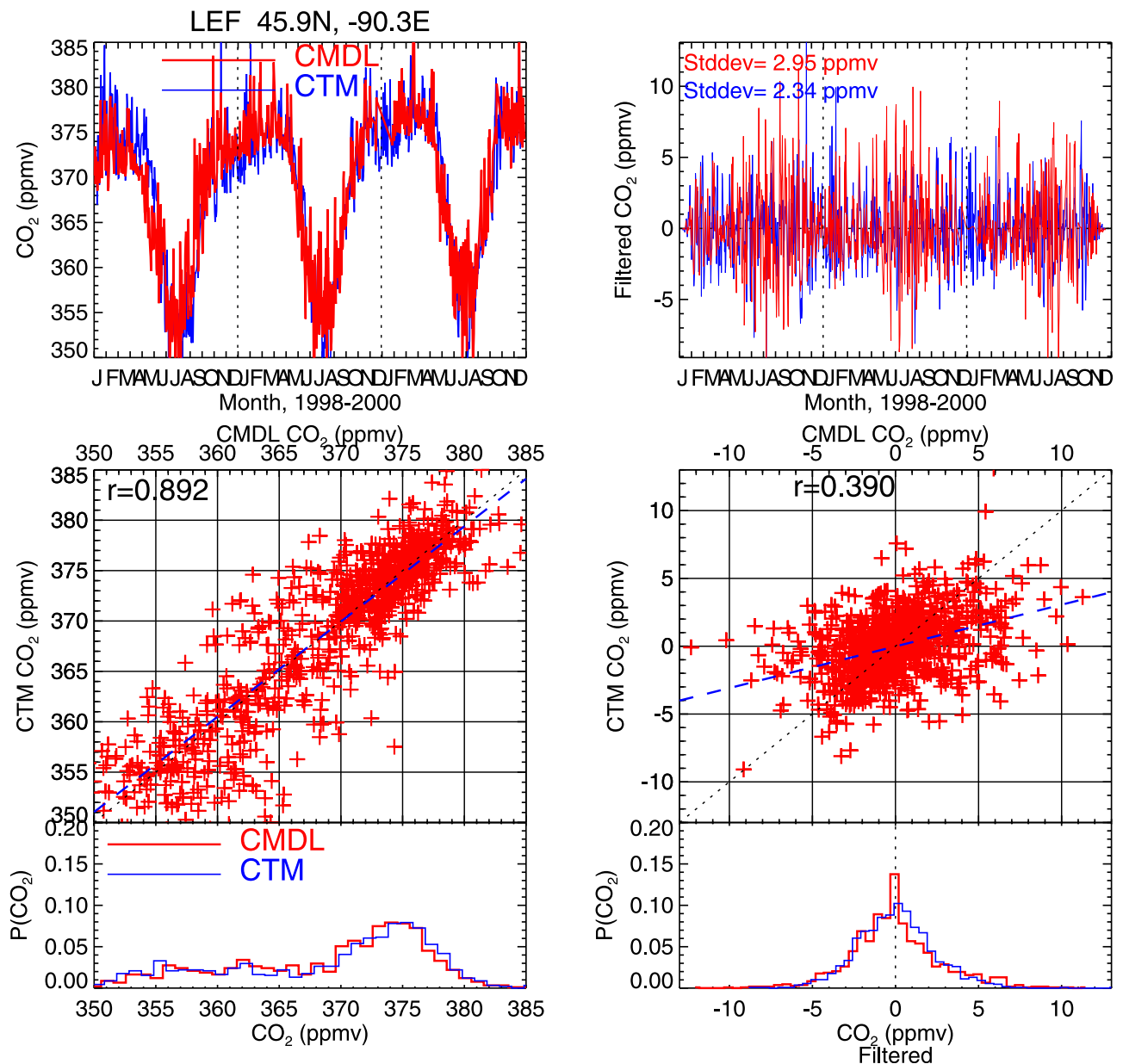


Figure 8a. Comparison of the synoptic-scale variability of daily mean atmospheric CO₂ in the model and continuous analyzer observations for LEF at 396 m AGL. (top left) Time series at the station for 1998–2000 with the model mean (blue) adjusted to that of the data (red). (top right) Time series of CO₂ after a high-pass filter (≈ 30 d, see Figure 9) has been applied. (middle) Observed versus modeled CO₂, (left) unfiltered and (right) filtered. (bottom) Normalized probability distributions of observed and modeled CO₂, unfiltered and filtered.

the seasonal cycle of atmospheric CO₂ in the Southern Hemisphere (based on a net source of 1.6 PG/yr and using different horizontal and seasonal distributions).

4.3.3. Southern Hemisphere

[38] The spatial and temporal patterns of atmospheric CO₂ in the southern hemisphere reflect the transported signal of NH-dominated processes (i.e., fossil fuel CO₂ emissions and terrestrial biosphere exchange) plus a contribution from the SH biosphere and oceans [e.g., Randerson *et al.*, 1997]. Comparison with observations throughout the SH mid and high latitudes shows that the seasonality of the CO₂ is in close agreement, but the amplitude is too large in

the model (Figures 6, 7, 8d, and 8e), similar to the results of Erickson *et al.* [1996]. The ocean sink has a maximum contribution to the seasonal cycle at the coastal site, PSA, where it is about one half of the amplitude seen in Figures 6 and 7. The biosphere cycle contributes the majority of the amplitude at other SH sites. The phase of the observations is very close to that of the model biosphere while the ocean signal leads the observations by about 3 months. The amplitude of the SH biosphere cycle may be overestimated, although in this simulation we cannot separate a lagged NH biosphere signal from the SH cycle. Should there be a bias in the magnitude or timing of the interhemispheric atmo-

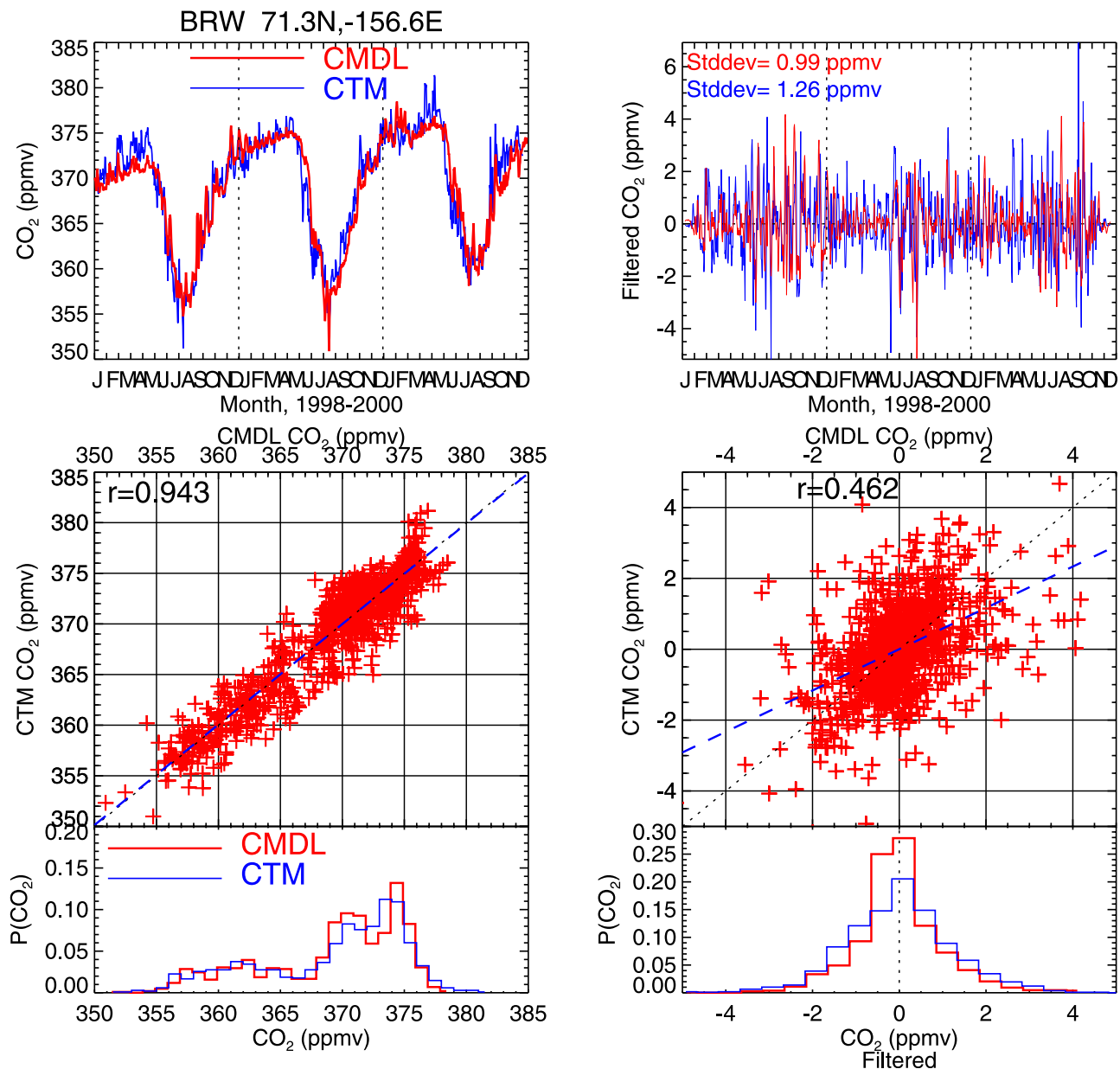


Figure 8b. Time series comparison for BRW as in Figure 8a.

spheric transport, this would result in the cycle of atmospheric CO₂ being different than that in the observations. Gurney *et al.* [2002] find less uptake in SH oceans than a priori estimates and suggest a greater seasonality for the SH ocean fluxes with uptake in summer and emission in winter, which would exacerbate the disagreement in the seasonal comparison here.

4.4. Trends in Atmospheric CO₂ Concentration

[39] The annual increase in the concentration of atmospheric CO₂ is highly variable from year to year, averaging about 1.6 ppmv/year (see, e.g., Conway *et al.* [1994] and updated through 2002 at <http://www.cmdl.noaa.gov/ccgg>). The increase for 1998–2000 is dominated by low CO₂ in Jan/Feb 1998 driving a larger trend than the decadal average at almost all sites. The model (with its annually steady state biosphere) trend is 1.69 ± 0.01 ppmv/year, consistent with

the source/sink inputs with little influence of interannual transport differences. The model trend varies by ± 0.4 across the measurement sites, related to the correlation between source sink/regions and prevailing weather patterns.

4.5. Synoptic to Daily Variations

[40] A major advantage of using analyzed winds for CO₂ transport simulations is the facility to compare to real-time variations in the observations at subseasonal scales. CO₂ variability contains information on synoptic scales that is indicative of the transport wind and surface source/sink variations, which have influenced any sampled air mass. Eventually we expect to make use of higher frequency and spatially resolved CO₂ measurements from space to improve estimates of sources and sinks. Here we analyze the time series of daily model output and observations from CMDL continuous analyzer sites. We do not expect the

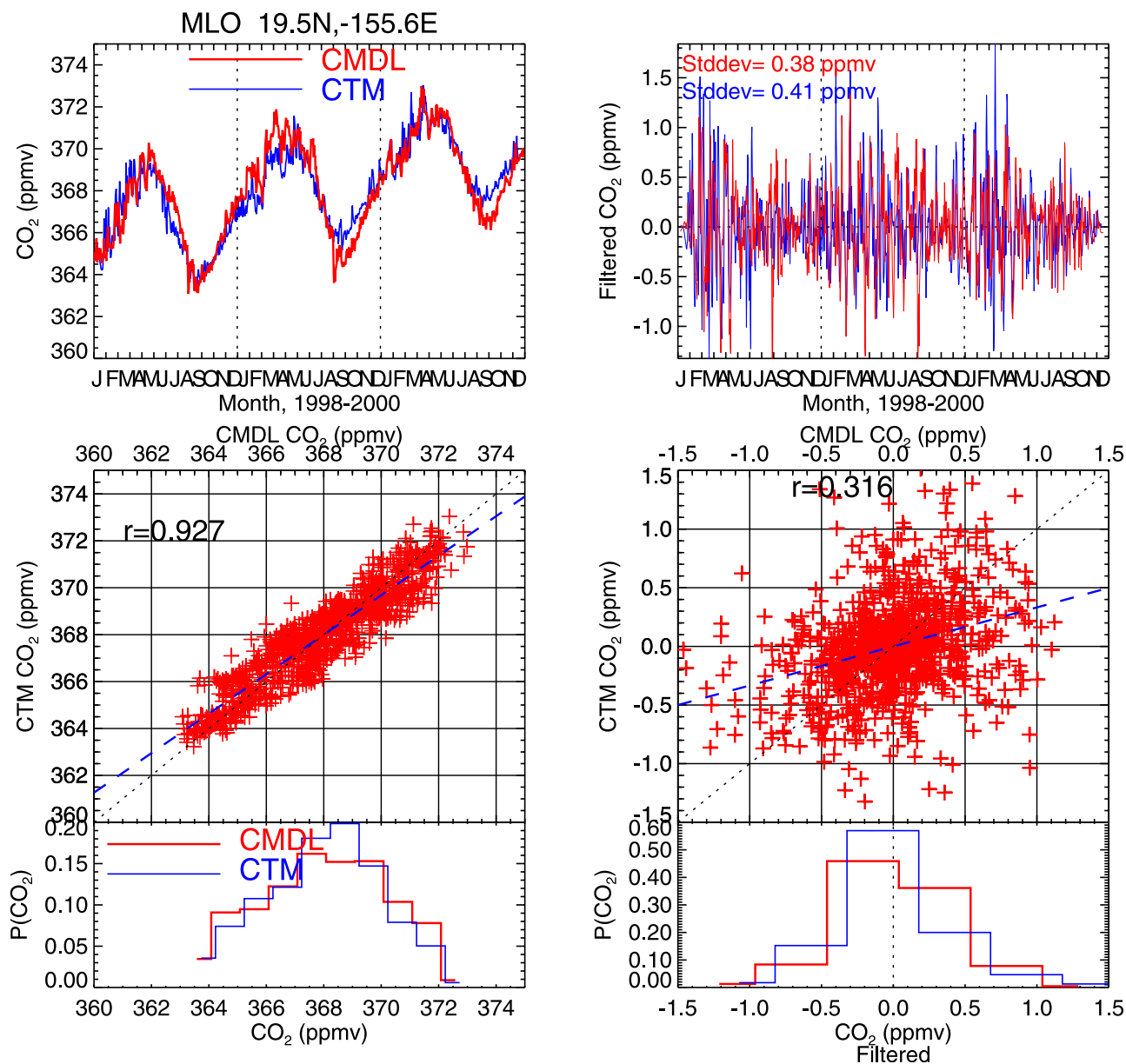


Figure 8c. Time series comparison for MLO as in Figure 8a.

model to capture all the details of the observed time series because of limited spatial resolution in the model and the fact that the model represents the surface forcing only in a climatological average sense (section 2.2). In situ observations have shown that CO₂ fluxes vary distinctly on relatively small scales (e.g., km) especially over land and that vegetation uptake/release responds strongly to regional fluctuations in meteorology (rainfall, temperature, cloudiness, etc) producing large CO₂ changes locally [Gerbig *et al.*, 2003]. The current model does not resolve processes at this level. We find, however, that use of the assimilated meteorological data enables the model to capture much of the observed daily variation in CO₂, which is driven to a large extent by transport variation.

[41] We start the discussion of synoptic and daily variation with the daily time series data from the Wisconsin tower site (LEF, Figure 8a), which is situated in the midst of

a mid latitude forest [Bakwin *et al.*, 1998]. As shown previously for the flask measurements, the seasonal cycle is well represented in the model. The right column of panels in Figure 8a shows that a significant correlation between the data and model remains even after the low-frequency variance is filtered from the time series. Variability at shorter timescales (<30 d) is driven by the changing weather systems and transport superimposed on the monthly varying surface sources and sinks for CO₂. The time series analysis indicates that many of the observed changes in CO₂ are captured by the model. We expect that using a surface source/sink distribution more tightly coupled to the actual meteorological fields would capture even more of the observed variation in the data. The standard deviation of the filtered time series and the power spectrum (Figure 9) show that model has less variance at higher frequencies than the observations, especially near 7 days, as might be

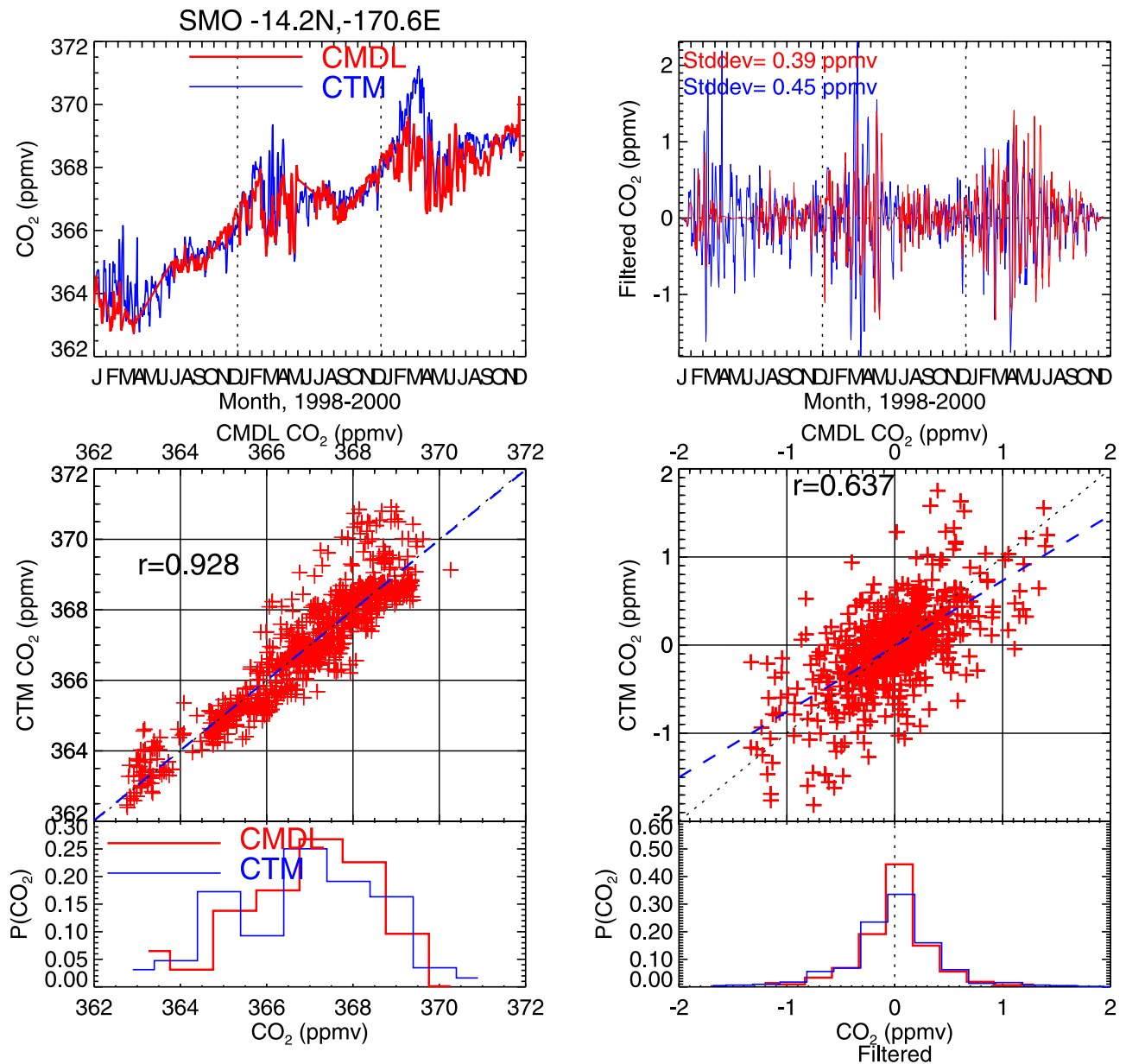


Figure 8d. Time series comparison for SMO as in Figure 8a. Correlation coefficient for the detrended time series comparison of observed versus model is 0.665.

expected for climatological surface fluxes that do not respond to changing weather. The timing of the transport events appears to be good in the model with a peak at zero lag in the cross correlation with the data (Figure 10). The power spectrum also shows the dominance of the annual seasonal cycle at periods larger than ~ 180 d (Figure 9). A 1.5-year time series analysis from another forested site (ITN, not shown) shows similar features to LEF with an even higher correlation (0.47) for the high pass filtered time series. The probability density functions (PDFs) for both the raw and filtered time series (Figure 8a) reaffirm the model's fidelity in simulating CO₂ variations from seasonal to daily times scales. Note that although the PDF mean value is constrained by the analysis procedure to be the same, the shapes are not. If we do a similar analysis (not shown) for the biospheric CO₂ only, the correlation of the filtered time

series is degraded, which means that the fossil fuel source has a significant influence on CO₂ at this site (the oceanic CO₂ contribution is nearly constant). Model fossil fuel CO₂ alone has much less variability than vegetation CO₂ since there is less spatial variability in the source, but advection of the fossil fuel source does contribute to the overall correlation between the model and data.

[42] The time series analysis at the Barrow, AK (BRW, Figure 8b), a high-latitude site remote from strong sources or sinks, shows similar seasonal variations to LEF, however, with much lesser variability on the shorter timescales. The correlation for the high-pass-filtered time series is relatively high, suggesting that transport variation plays a major role at this site. We note that the power spectrum (Figure 9) shows the model has more variance than the data at high frequency and suspect that this is a result of the admission

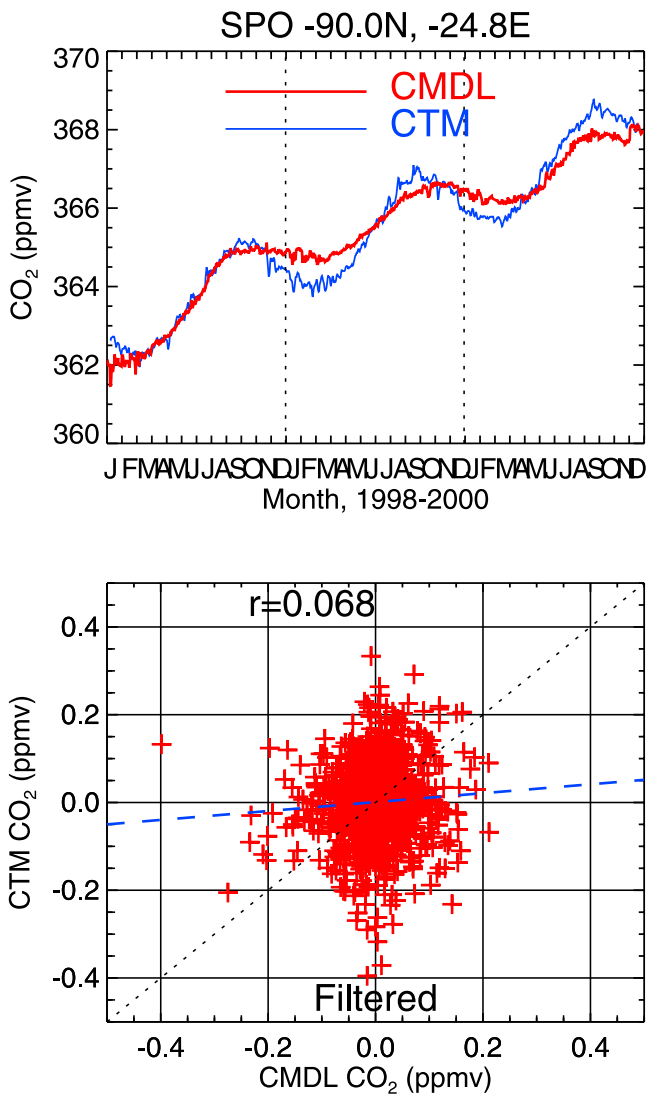


Figure 8e. Time series comparison for SPO as in Figure 8a except only raw time series and filtered correlation plots are shown.

criteria for the data. The data protocol accepts samples only from wind directions not influenced by local sources at BRW [Peterson *et al.*, 1986]. The PDFs again show the model's fidelity in simulating CO₂ variations over a range of times scales (Figure 8b). The data and model show a double peak in the PDF near 373 ppmv that results from the annual increase on top of the seasonal maximum. In analysis (not shown) for the biospheric CO₂ only, most diagnostics are similar but the histogram does not have a minimum near 373 ppmv. For the high-frequency (filtered) data, the model tends to spread the PDF relative to the data consistent with the higher variance in the power spectrum and less sharply peaked lag correlation (Figure 10).

[43] The CO₂ variation at MLO (Figure 8c), a remote mid-oceanic site in the free troposphere, is strongly influenced by transport of the terrestrial biosphere CO₂ and the fossil fuel combustion source. The MLO seasonal cycle in the model is slightly underestimated as seen from the time series peak-to-peak variation, the data-model cross plot fit

(Figures 8c and 10), comparison of the spectrum at periods >100 d (Figure 9), and the model PDF that is too tight (Figure 8c). At periods <30 days the level of variability is much less than the higher-latitude surface sites discussed above. The model has high-pass variance that is similar to the observations (S.D. = 0.40, 0.39, respectively) but the variations are not particularly well correlated ($r = 0.32$). We suspect that the lack of event correlation is related to the model parameterization of convective transport from the surface sources/sinks to the midtroposphere at MLO. Sub-grid-scale convective transport in the global model repre-

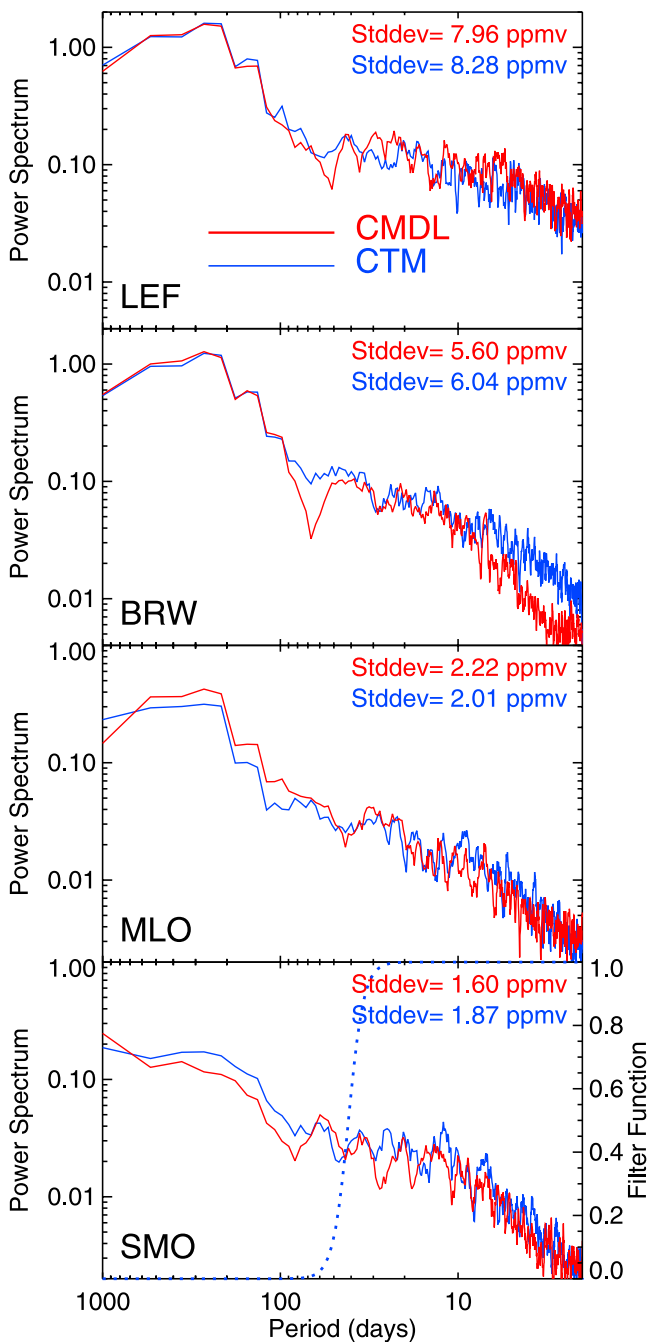


Figure 9. Power spectra of the observations and model time series (unfiltered) from Figures 8a–8e, along with the high-pass filter function.

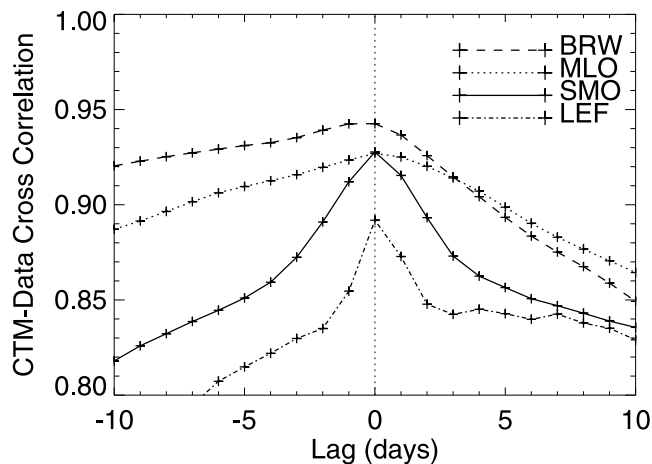


Figure 10. Data-model cross correlations as a function of lag in days, from the unfiltered time series of Figures 8a–8e. For the SMO detrended time series, the correlation maximum is 0.665, but it is even more strongly peaked at lag = 0 than that shown.

sents convection in a statistical sense, but not the details of individual convective events. Future DAS convective model developments will hopefully improve these correlations.

[44] The site at SMO (Figure 8d), a tropical oceanic surface site, has a small seasonal cycle, and the long-period variations are driven mainly by the annual increase. SMO also shows strong synoptic variability particularly in the northern winter-spring months. At periods <30 days, the model and observed spectra are similar (Figure 9) and the event correlation is high ($r = 0.64$) in spite of some missing data in spring of 1998. Much of the synoptic variation at this site is related to the seasonal movement of the ITCZ, which is resolved well by the transport meteorology. The variability of atmospheric CO₂ is large in the NH winter season when the ITCZ is displaced to the South and SMO comes under the influence of the NH sources. During NH summer the ITCZ is well north of SMO and the site is influenced by the relatively less variable CO₂ characteristic of the SH. Most model-data correlation and much of the variance at timescales <30 days is produced by the fossil fuel component of the CO₂. What little seasonal cycle exists is driven mainly by the model fossil fuel and ocean components, with the vegetation source correlation with data near zero. The seasonal maxima in the model are overestimated as seen in the unfiltered time series, correlation plot, and spectrum at longer periods suggesting that either the transport is too vigorous and/or the Northern Hemisphere net source is too large as has been inferred previously.

[45] The remote, elevated South Pole (SPO) station has a small seasonal cycle on top of the annual increase. As above the seasonal cycle in the model is larger than the data. Variance at shorter timescales is very small and largely represents uncorrelated noise in the measurements (Figure 8e).

[46] These time series comparisons between the assimilation-based model and continuous analyzer data show that there is significant information content at shorter timescales

than is typically exploited in models for CO₂ source/sink inversions, at least in some regions [Law *et al.*, 2002]. At several sites nearly half the variance in atmospheric CO₂ concentrations is due to meteorological variability superimposed on the climatological source/sink distributions. We expect to build on these comparisons to better constrain the distributions of sources and sinks and to utilize the potential of new space-based measurement systems.

5. Future Directions

[47] The study presented here motivates several avenues of future work. One next step is to employ higher-resolution, more realistic representations of the terrestrial biosphere flux using a terrestrial biosphere model. The forward model provides a basis for direct comparison of the computed CO₂ distributions to evaluate the quality of the biosphere models. We hope to support field programs (e.g., North American Carbon Program) and possibly provide boundary conditions for nested high-resolution (e.g., mesoscale) models of atmospheric CO₂ dynamics that will connect local process studies to the global carbon budget. We are also putting CO₂ transport on line in the GCM working toward a long-term goal of a coupled atmosphere-ocean-land model for carbon and climate.

[48] The comparisons with observations provide a baseline that can be used to evaluate future model developments, e.g., boundary layer parameterization, convective fluxes, model gridding, etc., and to quantify the impact of their uncertainties on global CO₂ transport simulation. In addition, we have begun using this modeling system in inverse modeling, the transport adjoint, and CO₂ data assimilation. As global satellite observations for CO₂ become available assimilation-based modeling will be required to exploit the increased coverage and temporal sampling offered by remote sensing.

[49] Finally, the model provides a test bed for examining measurement system (e.g., the CO₂ laser sounder) requirements and in conjunction with inverse calculations, their impact on inference of surface fluxes. Future modeling projects will include simulations of quantities such as aerosol and clouds that affect our ability to measure the CO₂ distribution from space. One goal of this work is to supply a more realistic model CO₂ atmosphere (e.g., Figure 2) to developers of satellite retrieval algorithms.

6. Summary and Conclusions

[50] We have described a global model (PCTM) for atmospheric CO₂ transport using the NASA FVDAS analyzed meteorological fields, including estimates of subgrid-scale transport. The global distribution of atmospheric CO₂ has been simulated for 1998–2000, using a set of specified surface sources and sinks including those from TransCom. The use of assimilated winds allows real-time, site-specific comparison of computed atmospheric CO₂ mixing ratios to data on a wide range of timescales. This constitutes the first steps to using FVDAS to infer CO₂ sources and sinks and ultimately to a fully coupled data assimilation system for carbon cycle processes.

[51] Analysis of the forward transport model diagnostics and comparison to results from previous model intercom-

parisons shows the quality of the model performance. The horizontal and vertical gradients in CO₂ and SF₆ are consistent with most models in the TransCom intercomparisons. The interhemispheric gradient in SF₆ is in reasonable agreement with observations, although the mixing time of the DAS-PCTM is a bit quicker (0.61 years) than most of the other models. The interhemispheric CO₂ gradient is overestimated compared to observations consistent with previous studies indicating that an additional sink for atmospheric CO₂ is required in the NH biosphere. The distribution of column integrated CO₂, a quantity that is a likely candidate for space-based global measurements, shows gradients on the order of several ppmv/1000 km exist in response to surface source/sink forcing. These distributions compose a first-order precision requirement for design of satellite-based remote sensing instruments.

[52] The amplitude and phase of the seasonal cycle of atmospheric CO₂ is in good agreement with the CMDL observation stations at NH mid to high latitudes. The seasonal cycle is driven by the strong influence of the terrestrial biosphere, indicating that the specified flux distributions are well represented. The NH summer minimum in the subtropics is too high in the model suggesting a stronger biosphere uptake may be needed at these latitudes. The amplitude of the model seasonal cycle is overestimated at most SH measurement sites. Both ocean and biosphere contribute to the computed excess.

[53] We find significant advantages in using the FVDAS analyzed winds when making synoptic-scale temporal comparisons to data. The horizontal distributions and time series of CO₂ variations reflect both the source sink distributions and the transport, which is closely constrained to actual weather observations. In tropical regions the model produces an accurate portrayal of the latitudinal movement of the ITCZ and associated atmospheric CO₂ changes. The model captures a significant amount of the synoptic-scale variability in comparison with daily observations, even using climatological source and sinks. This leads us to expect that the DAS will form a solid basis for inversion methods to estimate surface source/sink relationships for specific time periods especially in combination with anticipated high-resolution data from remote sensing.

[54] **Acknowledgments.** We would like to acknowledge the contributions and helpful discussions of Arlyn Andrews, Jim Collatz, and J. Mao, as well as comments from P. Tans and two anonymous reviewers. The observational CO₂ data are provided by the NOAA CMDL Carbon Cycle Cooperative Global Air Sampling Network. The distributions of biomass burning emissions were provided by J. A. Logan and R. M. Yevich. DE acknowledges support from the Center for Computational Sciences at Oak Ridge National Laboratory, which is supported by the Office of Science of the U.S. Department of Energy under contract DE-AC05-00OR22725. Funding support has been provided by NASA Carbon Cycle Science.

References

- Andres, R. J., G. Marland, I. Fung, and E. Matthews (1996), Distribution of carbon dioxide emissions from fossil fuel consumption and cement manufacture, 1950–1990, *Global Biogeochem. Cycles*, *10*, 419–429.
- Bakwin, P. S., P. P. Tans, D. F. Hurst, and C. L. Zhao (1998), Measurements of carbon dioxide on very tall towers: Results of the NOAA/CMDL program, *Tellus, Ser. B*, *50*, 401–415.
- Bousquet, P., P. Ciais, P. Peylin, M. Ramonet, and P. Monfray (1999), Inverse modeling of annual atmospheric CO₂ sources and sinks: 1. Method and control inversion, *J. Geophys. Res.*, *104*, 26,161–26,193.
- Bousquet, P., et al. (2000), Regional changes in carbon dioxide fluxes of land and ocean since 1980, *Science*, *290*, 1342–1346.
- Cohn, S. E., A. da Silva, J. Guo, M. Sienkiewicz, and D. Lamich (1998), Assessing the effects of data selection with the DAO physical-space statistical analysis system, *Mon. Weather Rev.*, *126*, 2913–2926.
- Conway, T. J., P. P. Tans, L. S. Waterman, K. W. Thoning, K. A. Masarie, and R. H. Gammon (1988), Atmospheric carbon dioxide measurements in the remote global troposphere, 1981–1984, *Tellus, Ser. B*, *40*, 81–115.
- Conway, T. J., P. P. Tans, L. S. Waterman, K. W. Thoning, D. R. Kitzis, K. A. Masarie, and N. Zhang (1994), Evidence for interannual variability of the carbon cycle from the National Oceanic and Atmospheric Administration/Climate Monitoring and Diagnostics Laboratory Global Air Sampling Network, *J. Geophys. Res.*, *99*, 22,831–22,855.
- Dargaville, R. J., R. M. Law, and F. Pribac (2000), Implications of interannual variability in atmospheric circulation on modeled CO₂ concentrations and source estimates, *Global Biogeochem. Cycles*, *14*, 931–943.
- Denning, A. S., I. Y. Fung, and D. A. Randall (1995), Latitudinal gradient of atmospheric CO₂ due to seasonal exchange with land biota, *Nature*, *376*, 240–243.
- Denning, A. S., et al. (1999), Three-dimensional transport and concentration of SF₆—A model intercomparison study (TransCom 2), *Tellus, Ser. B*, *51*, 266–297.
- Douglas, A. R., and S. R. Kawa (1999), Contrast between 1992 and 1997 high-latitude spring Halogen Occlusion Experiment observations of lower stratospheric HCl, *J. Geophys. Res.*, *104*, 18,739–18,754.
- Douglas, A. R., M. R. Schoeberl, R. B. Rood, and S. Pawson (2003), Evaluation of transport in the lower tropical stratosphere in a global chemistry and transport model, *J. Geophys. Res.*, *108*(D9), 4259, doi:10.1029/2002JD002696.
- Duncan, B. N., R. V. Martin, A. C. Staudt, R. Yevich, and J. A. Logan (2003), Interannual and seasonal variability of biomass burning emissions constrained by satellite observations, *J. Geophys. Res.*, *108*(D2), 4100, doi:10.1029/2002JD002378.
- Enting, I. G., and J. V. Mansbridge (1991), Latitudinal distribution of sources and sinks of CO₂: Results of an inversion study, *Tellus, Ser. B*, *43*, 156–170.
- Erickson, D. J., III, P. J. Rasch, P. P. Tans, P. Friedlingstein, P. Ciais, E. Maier-Reimer, K. Kurz, C. A. Fischer, and S. Walters (1996), The seasonal cycle of atmospheric CO₂: A study based on the NCAR Community Climate Model (CCM2), *J. Geophys. Res.*, *101*, 15,079–15,097.
- Fan, S., M. Gloor, J. Mahlman, S. Pacala, J. Sarmiento, T. Takahashi, and P. Tans (1998), A large terrestrial carbon sink in North America implied by atmospheric and oceanic carbon dioxide data and models, *Science*, *282*, 442–446.
- Fung, I., K. Prentice, E. Matthews, J. Lerner, and G. Russell (1983), Three-dimensional tracer model study of atmospheric CO₂: Response to seasonal exchanges with the terrestrial biosphere, *J. Geophys. Res.*, *88*, 1281–1294.
- Gerbig, C., J. C. Lin, S. C. Wofsy, B. C. Daube, A. E. Andrews, B. B. Stephens, P. S. Bakwin, and C. A. Grainger (2003), Toward constraining regional-scale fluxes of CO₂ with atmospheric observations over a continent: 1. Observed spatial variability from airborne platforms, *J. Geophys. Res.*, *108*(D24), 4756, doi:10.1029/2002JD003018.
- Gurney, K. G., et al. (2002), Towards robust regional estimates of CO₂ sources and sinks using atmospheric transport models, *Nature*, *415*, 626–630.
- Gurney, K. G., et al. (2003), TransCom 3 CO₂ inversion intercomparison: 1. Annual mean control results and sensitivity to transport and prior flux information, *Tellus, Ser. B*, *55*, 555–579.
- Hack, J. J. (1994), Parameterization of moist convection in the National Center for Atmospheric Research community climate model (CCM2), *J. Geophys. Res.*, *99*, 5551–5568.
- Heimann, M., and C. D. Keeling (1989), A three-dimensional model of atmospheric CO₂ transport based on observed winds: 2. Model description and simulated tracer experiments, in *Aspects of Climate Variability in the Pacific and the Western Americas*, *Geophys. Monogr. Ser.*, vol. 55, pp. 237–275, edited by D. H. Peterson, AGU, Washington, D. C.
- Holtlag, A. A. M., and B. A. Boville (1993), Local versus non-local boundary layer diffusion in a global climate model, *J. Clim.*, *6*, 1825–1842.
- Intergovernmental Panel on Climate Change (IPCC) (2001), *Climate Change 2001: Synthesis Report, Third Assessment Report of the Intergovernmental Panel on Climate Change*, Cambridge Univ. Press, New York.
- Joiner, J., and L. Rokke (2000), Variational cloud-clearing with TOVS data, *Q. J. R. Meteorol. Soc.*, *126*, 725–748.
- Kiehl, J. T., J. J. Hack, G. B. Bonan, B. A. Boville, D. L. Williamson, and P. J. Rasch (1998), The National Center for Atmospheric Research Community Climate Model: CCM3, *J. Clim.*, *11*, 1131–1149.
- Kuang, Z., J. Margolis, G. Toon, D. Crisp, and Y. Yung (2002), Spaceborne measurements of atmospheric CO₂ by high-resolution NIR spectrometry of reflected sunlight: An introductory study, *Geophys. Res. Lett.*, *29*(15), 1716, doi:10.1029/2001GL014298.

- Langenfelds, R. L., R. J. Francey, B. C. Pak, L. P. Steele, J. Lloyd, C. M. Trudinger, and C. E. Allison (2002), Interannual growth rate variations of atmospheric CO₂ and its $\delta^{13}\text{C}$, H₂, CH₄, and CO between 1992 and 1999 linked to biomass burning, *Global Biogeochem. Cycles*, *16*(3), 1048, doi:10.1029/2001GB001466.
- Law, R. M., et al. (1996), Variations in modeled atmospheric transport of carbon dioxide and the consequences for CO₂ inversions, *Global Biogeochem. Cycles*, *10*, 783–796.
- Law, R. M., P. J. Rayner, L. P. Steele, and I. G. Enting (2002), Using high temporal frequency data for CO₂ inversions, *Global Biogeochem. Cycles*, *16*(4), 1053, doi:10.1029/2001GB001593.
- Li, Q. B., et al. (2002), Transatlantic transport of pollution and its effects on surface ozone in Europe and North America, *J. Geophys. Res.*, *107*(D13), 4166, doi:10.1029/2001JD001422.
- Lin, S. J., and R. B. Rood (1996), Multidimensional flux-form semi-Lagrangian transport schemes, *Mon. Weather Rev.*, *124*, 2046–2070.
- Mao, J., and S. R. Kawa (2004), Sensitivity studies for space-based measurement of atmospheric total column carbon dioxide using reflected sunlight, *Appl. Opt.*, *43*, 914–927.
- McPeters, R. D., and G. J. Labow (1996), An assessment of the accuracy of 14.5 years of Nimbus 7 TOMS version 7 ozone data by comparison with the Dobson network, *Geophys. Res. Lett.*, *23*, 3695–3698.
- Nakazawa, T., K. Miyashita, S. Aoki, and M. Tanaka (1991), Temporal and spatial variations of upper tropospheric and lower stratospheric carbon dioxide, *Tellus, Ser. B*, *43*, 106–117.
- Nielsen, J. E., and A. R. Douglass (2001), Simulation of bromoform's contribution to stratospheric bromine, *J. Geophys. Res.*, *106*, 8089–8100.
- O'Brien, D. M., and P. J. Rayner (2002), Global observations of carbon budget: 2. CO₂ concentrations from differential absorption of reflected sunlight in the 1.61 m band of CO₂, *J. Geophys. Res.*, *107*(D18), 4354, doi:10.1029/2001JD000617.
- Pak, B. C., and M. J. Prather (2001), CO₂ source inversions using satellite observations of the upper troposphere, *Geophys. Res. Lett.*, *28*, 4571–4574.
- Peterson, J. T., W. D. Komhyr, L. S. Waterman, R. H. Gammon, K. W. Thoning, and T. J. Conway (1986), Atmospheric CO₂ variations at Barrow, Alaska, 1973–1982, *J. Atmos. Chem.*, *4*, 491–510.
- Peylin, P., D. Baker, J. Sarmiento, P. Ciais, and P. Bousquet (2002), Influence of transport uncertainty on annual mean and seasonal inversions of atmospheric CO₂ data, *J. Geophys. Res.*, *107*(D19), 4385, doi:10.1029/2001JD000857.
- Prather, M. J., et al. (1987), Chemistry of the global troposphere fluorocarbons as tracers of air motion, *J. Geophys. Res.*, *92*, 6579–6613.
- Randerson, J. T., et al. (1997), The contribution of terrestrial sources and sinks to trends in the seasonal cycle of atmospheric carbon dioxide, *Global Biogeochem. Cycles*, *11*, 535–560.
- Rayner, P. J., and D. M. O'Brien (2001), The utility of remotely sensed CO₂ concentration data in surface source inversions, *Geophys. Res. Lett.*, *28*, 175–178.
- Rayner, P. J., R. M. Law, and R. Dargaville (1999), The relationship between tropical CO₂ fluxes and the El Niño-Southern Oscillation, *Geophys. Res. Lett.*, *26*, 493–496.
- Rotman, D. A., et al. (2001), Global Modeling Initiative assessment model: Model description, integration, and testing of the transport shell, *J. Geophys. Res.*, *106*, 1669–1691.
- Schimel, D., et al. (2000), Contribution of increasing CO₂ and climate to carbon storage by ecosystems in the United States, *Science*, *287*, 2004–2006.
- Schimel, D. S., et al. (2001), Recent patterns and mechanisms of carbon exchange by terrestrial ecosystems, *Nature*, *414*, 169–172.
- Taguchi, S. (1996), A three-dimensional model of atmospheric CO₂ transport based on analyzed winds: Model description and simulation results for TRANSCOM, *J. Geophys. Res.*, *101*, 15,099–15,109.
- Takahashi, T., R. A. Feely, R. Weiss, R. H. Wanninkhof, D. W. Chipman, S. C. Sutherland, and T. T. Takahashi (1997), Global air-sea flux of CO₂: An estimate based on measurements of sea-air pCO₂ difference, *Proc. Natl. Acad. Sci. U. S. A.*, *94*, 8929.
- Takahashi, T., R. H. Wanninkhof, R. A. Feely, R. F. Weiss, D. W. Chipman, N. Bates, J. Olafsson, C. Sabine, and S. C. Sutherland (1999), Net sea-air CO₂ flux over the global oceans: An improved estimate based on the sea-air pCO₂ difference, paper presented at 2nd CO₂ in Oceans Symposium, Cent. for Global Environ. Res. Natl. Inst. for Environ. Stud., Tsukuba, Japan.
- Tans, P. P., I. Y. Fung, and T. Takahashi (1990), Observational constraints on the global atmospheric CO₂ budget, *Science*, *247*, 1431–1438.
- Thoning, K. W., P. P. Tans, and W. D. Komhyr (1989), Atmospheric carbon dioxide at Mauna Loa Observatory: 2. Analysis of the NOAA/GMCC data, 1974–1985, *J. Geophys. Res.*, *94*, 8549–8565.
- Zhang, G. J., and N. A. McFarlane (1995), Sensitivity of climate simulations to the parameterization of cumulus convection in the Canadian climate center general-circulation model, *Atmos. Ocean*, *33*, 407–446.

D. J. Erickson III, Oak Ridge National Laboratory, Oak Ridge, TN 37831, USA.

S. R. Kawa, NASA Goddard Space Flight Center, Greenbelt, MD 20771, USA. (stephan.r.kawa@nasa.gov)

S. Pawson, Goddard Earth Science and Technology Center, Baltimore, MD 20771, USA.

Z. Zhu, Science Systems and Applications, Inc, Lanham, MD 20706, USA.